SPECIAL FEATURE: PERSPECTIVE

Layerless fabrication with continuous liquid interface production

Rima Janusziewicz[a], John R. Tumbleston[b], Adam L. Quintanilla[c], Sue J. Mecham[a], and Joseph M. DeSimone[a,b,c,1]

Edited by John A. Rogers, University of Illinois at Urbana–Champaign, Urbana, IL, and approved August 23, 2016 (received for review May 1, 2016)

Despite the increasing popularity of 3D printing, also known as additive manufacturing (AM), the technique has not developed beyond the realm of rapid prototyping. This confinement of the field can be attributed to the inherent flaws of layer-by-layer printing and, in particular, anisotropic mechanical properties that depend on print direction, visible by the staircasing surface finish effect. Continuous liquid interface production (CLIP) is an alternative approach to AM that capitalizes on the fundamental principle of oxygen-inhibited photopolymerization to generate a continual liquid interface of uncured resin between the growing part and the exposure window. This interface eliminates the necessity of an iterative layer-by-layer process, allowing for continuous production. Herein we report the advantages of continuous production, specifically the fabrication of layerless parts. These advantages enable the fabrication of large overhangs without the use of supports, reduction of the staircasing effect without compromising fabrication time, and isotropic mechanical properties. Combined, these advantages result in multiple indicators of layerless and monolithic fabrication using CLIP technology.

stereolithogaphy | continuous liquid interface production | 3D printing | additive manufacturing | isotropic properties

Additive manufacturing (AM), or 3D printing, is a growing field that employs the selective layering of material to build a part, which has distinct advantages compared with subtractive manufacturing (1). The benefits of additive over subtractive manufacturing are numerous and include unlimited design space, freedom of complex geometries, and reduction of waste by-products (2). Significant advancements were made to AM in the 1980s with the development of the stereolithography (SL) apparatus, a platform that uses the exposure of a rastering UV laser to selectively solidify a resin through a photopolymerization process in a top-down manner (3). The method has since been modified to solidify in a bottom-up process through the use of a digital light projection (DLP) chip that eliminates the rastering laser. The process of bottom-up SL begins with a computer-aided design (CAD) file that is then converted into a series of 2D renderings using a method called "slicing" (Fig. 1*A*). The original object is then reconstructed in a layer-by-layer manner by reproducing these 2D renderings, one slice at a time. This process is done iteratively whereby a photoactive resin is selectively exposed to UV light through a transparent substrate, allowing for selective photopolymerization corresponding to a specific slice shape (4). Once the slice has been exposed, a series of mechanical steps of separation, recoating, and repositioning follow (Fig. 1*B*) to allow for subsequent exposure.

The polymeric materials used in the SL process are known to have intrinsic properties that are a function of the chemical structure, molecular weight, and topology (3). Printed part properties differ from intrinsic polymeric properties because they are a result of both the material and the process used to produce the part. These differences are important with respect to the production of fibers and films made from thermoplastics, where morphology and anisotropy can be imparted as a function of the process (5, 6). The physical properties of thermosets are complicated further because the polymer structure, molecular weight between cross-links, and topology are formed during the processing of the part, and thus intrinsic properties and the part properties are inextricably entwined. Although the SL platform has proved useful in the biomedical (7–10) and microfluidic

[a]Department of Chemistry, University of North Carolina at Chapel Hill, Chapel Hill, NC 27599; [b]Carbon, Inc., Redwood City, CA 94063; and [c]Department of Chemical and Biomolecular Engineering, North Carolina State University, Raleigh, NC 27695

Author contributions: R.J., S.J.M., and J.M.D. designed research; R.J. performed research; R.J., J.R.T., and A.L.Q. contributed new reagents/analytic tools; R.J., J.R.T., A.L.Q., and S.J.M. analyzed data; and R.J. and S.J.M. wrote the paper.

Conflict of interest statement: J.R.T. and J.M.D. have an equity stake in Carbon, Inc., which is a venture-backed manufacturer of continuous liquid interface production equipment. Continuous liquid interface production is the subject of patent protection including issued US patents 9,205,601, 9,211,678, and 9,216,546.

This article is a PNAS Direct Submission.

[1]To whom correspondence should be addressed. Email: desimone@email.unc.edu.

This article contains supporting information online at www.pnas.org/lookup/suppl/doi:10.1073/pnas.1605271113/-/DCSupplemental.

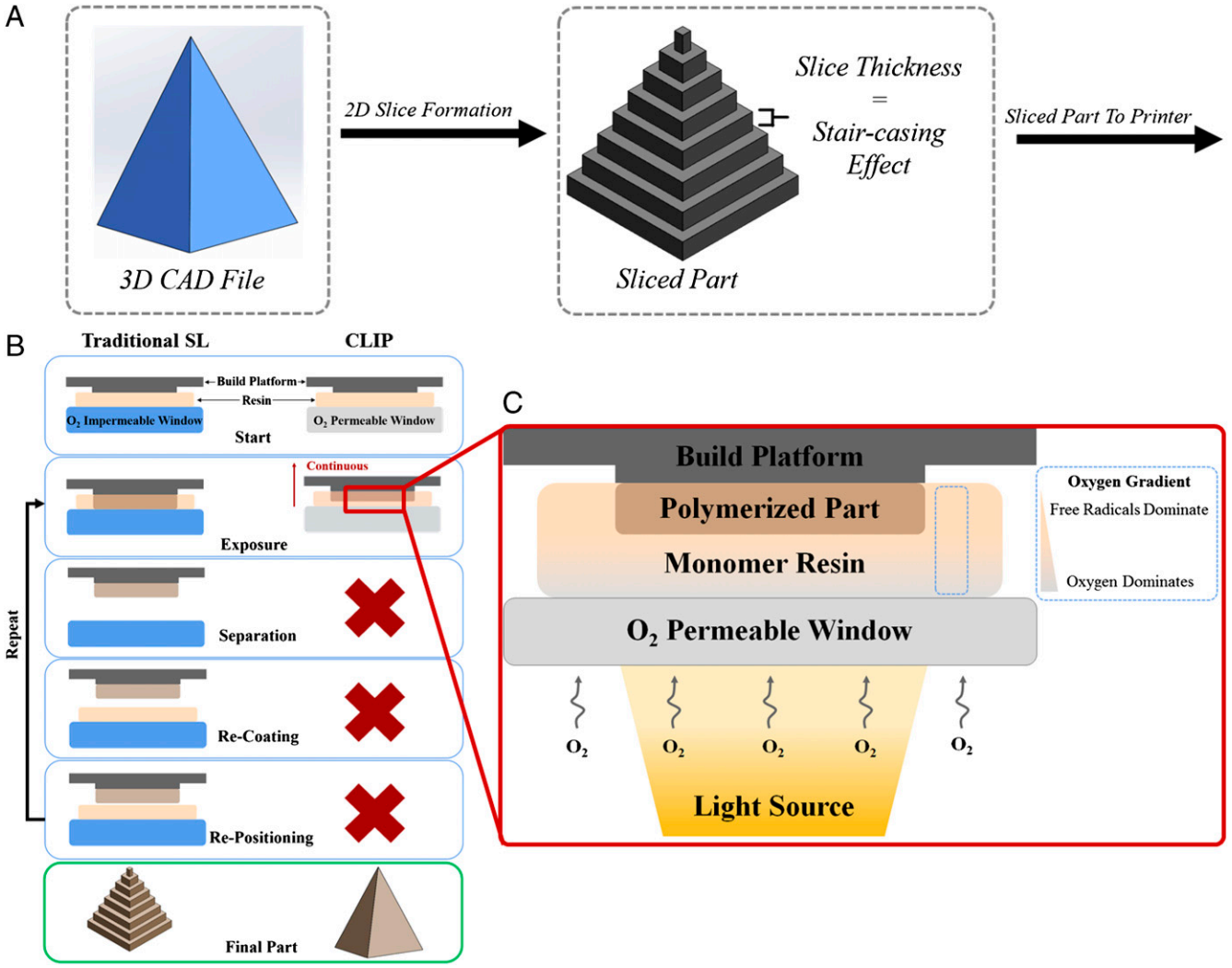

Fig. 1. Basic step comparison of traditional SL to CLIP. (*A*) Generation and slicing of a 3D CAD file are necessary steps for both the SL and CLIP platforms. (*B*) Traditional SL requires five fundamental steps to print a part: build elevator placement on resin (*i*), UV exposure to selectively cure resin (*ii*), separation of cured resin from the O_2-impermeable window (*iii*), mechanical recoating of resin (*iv*), and, finally, repositioning of the build elevator (*v*) to repeat the process until the part is fully printed. CLIP uses a constant liquid interface enabled by the O_2-permeable window, which eliminates the need for steps (*ii*, *iii*, and *iv*). (*C*) Schematic of the dead zone (DZ) produced by the presence of oxygen and the generation of free radicals upon UV exposure. Within the DZ there exists a concentration gradient of O_2 whereas within the bulk there exist gradient light intensity and, to some degree, conversion before vitrification (34).

fields (11–13), significant challenges are innate to this layer-by-layer approach. These challenges include limited materials and material properties, dimensional accuracy, shape and part orientation optimization, slicing, and speed (14–16).

A specific challenge regarding SL is the anisotropic bulk mechanical properties in the direction of the axis of printing when using acrylate-based resin systems (17) and the staircasing effect on curved or angled surfaces (Fig. 1*A*) (18–22). The magnitude of this staircasing effect is dictated by the thickness of the process slice and results in a nonideal loss of part resolution (23). Existing AM platforms produce this staircasing effect on the surface of the fabricated part, regardless of orientation; however, it is most profoundly noticed on sloped features. This effect can be countered by reduction of the slice thickness in the 2D rendering and implemented by either finely slicing the part throughout or using a technique called adaptive slicing, which enables a user to select regions for thinner slicing (24). These methods, however, result in a significantly increased build time given the number of mechanical resin renewal steps between each layer exposure. Some epoxy-based resin systems also represent an alternative to overcoming anisotropic mechanical properties (25, 26); however, the kinetics are not completely "switch-like" in the presence of UV light because the polymer will continue to react even after UV exposure is terminated (27). Because of this residual reactivity, material properties are often dependent on slice thickness, where thinner slicing allows for more interlayer cohesion to occur (28). Therefore, the layer-by-layer approach has an intrinsic trade-off between part quality and part build time. It can be concluded that the primary cause for the limitation of the SL platform and AM technologies within the field of rapid manufacturing can be attributed to the layer-by-layer approach.

Recently, continuous liquid interface production (CLIP) was introduced to circumvent these inherent obstacles and expand the adoption of AM (29). CLIP relies on the inhibition of free radical photopolymerization in the presence of atmospheric oxygen. Oxygen can quench either the excited-state photoinitiator or

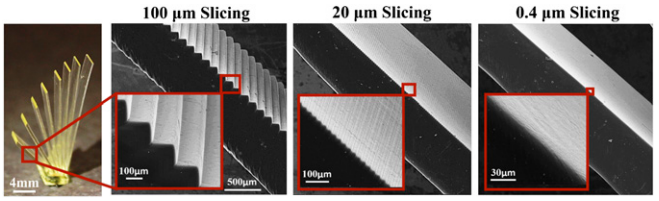

Fig. 2. Open book benchmark fabricated with changing slicing conditions. ESEM micrographs obtained by imaging the 20° page of the open book benchmark under the three slice thicknesses.

form a peroxide upon interaction with a free radical of a propagating chain (Eqs. **S1**–**S5**) (30–34). Therefore, performing SL on an oxygen-permeable build window results in the formation of a dead zone, or a region of uncured liquid resin (29). Polymerization and solidification is achieved once the O_2 has been depleted such that the kinetics of propagation (k_p[monomer]) are in competitive balance with the kinetics of radical generation and subsequent O_2 inhibition ($k_i[O_2]$) (34, 35). The dead zone, present throughout the fabrication process, represents the uncured liquid layer between the growing part and the window and is the defining difference between CLIP and traditional SL (Fig. 1*B*). As shown in Fig. 1*C*, the presence of the dead zone allows for part production, resin renewal, and build elevator movement to occur simultaneously, as opposed to the discrete steps of SL. This mechanism eliminates the traditional resolution and fabrication speed trade-off because of the continuity of the fabrication process. At the molecular level, the kinetic competition between oxygen inhibition and free radical generation, once reached, is maintained throughout the fabrication of the part (34). Conversely, in traditional SL all reactions are confined to the solidification of a single layer, which occurs over and over throughout the printing. Herein, we demonstrate that the CLIP method of part fabrication leads to monolithic production resulting in isotropic mechanical properties and enables reduction of the staircasing effect without affecting the overall build time.

Discussion

The field of AM has incorporated several benchmark structures to evaluate the performance of different platforms that vary depending on the aspect of the platform being probed (36). The open book benchmark was designed to evaluate a platform's ability to print large overhangs at different angles with or without supports, alluding to the mechanical integrity of the final part (37). The open book benchmark was adapted for the CLIP platform and fabricated with changing input slice thickness to isolate and minimize the observed staircasing effect. Because of the continuous nature of the resin renewal mechanism for CLIP, parts with different slice thicknesses (100, 20, and 0.4 μm) were fabricated with the same build speed of 40 mm/h and yielded the same build time. By decreasing the slice thickness, the smooth slope feature of the open book could be better approximated, thus enabling the reduction of the staircasing effect, illustrated in Fig. 2, independent of the traditional trade-off with build time. Because the formation of the dead zone is kinetically driven, parameter optimization of light intensity, build speed, and weight percent UV absorber was necessary. Briefly, the cure thickness of the resin was calculated under static conditions using methods outlined in Tumbleston et al. (29) to yield initial fabrication parameters. However, because the CLIP process is dynamic, adjustments were necessary to properly maintain the dead zone throughout the fabrication process (*Supporting Information* and Fig. S1). The resulting surface topology therefore is imparted solely by the treatment of the CAD file, rather than the fabrication process itself. Furthermore, the sloped "pages" of the open book are freely extending in space and are fabricated without supports, partly aided by the bottom-up build approach. Conventional AM approaches either lack chemical cohesion between layers or impart a mechanical strain on the part in the separation step, thus preventing the fabrication of large overhangs without additional aids in the form of supports (37, 38). The continuity of fabrication enabled by CLIP allows for the reduction of the staircasing effect without affecting build time and results in a part with the mechanical integrity to support large overhangs.

Two "pages" of the open book were evaluated using optical laser scanning (OLS) noncontact profilometer imaging, shown in Fig. 3, to quantify the change in surface topology with respect to changing slicing parameters. Two parameters of surface roughness were used: arithmetical mean deviation (R_a) and mean length (R_{Sm}). The orientation of the slicing direction relative to the analysis direction indicates that the R_{Sm} parameter yields a frequency of length measurement and thus the distance between steps, whereas the R_a parameter denotes a mean depth of the steps. Illustrations of the two parameters as they apply to the 20° open book page are shown in Fig. 4*A*. The R_a parameter was measured for both the 90° and 20° pages to determine the effect of slice thickness on surface topology. For the part to be monolithic, the R_a of the 90° page surface should be independent of slicing, given that the exposure frame remains unchanged throughout its fabrication, illustrated in Fig. 4*B*. As shown in Table 1, R_a remains constant for the 90° page yet scales with input slice thickness for the 20° page, supporting the claim of layerless fabrication.

To quantitatively validate the causal relationship between slice thickness and observed staircasing effect, the observed step height was determined. Previous work has explored the measurement of step height using only the R_a parameter (39–41). These measurements are not suited for comparing a large range of slice thickness given the necessity to control the number of sampling points. An alternative method for determining experimental step height was developed using the R_{Sm} parameter obtained through OLS

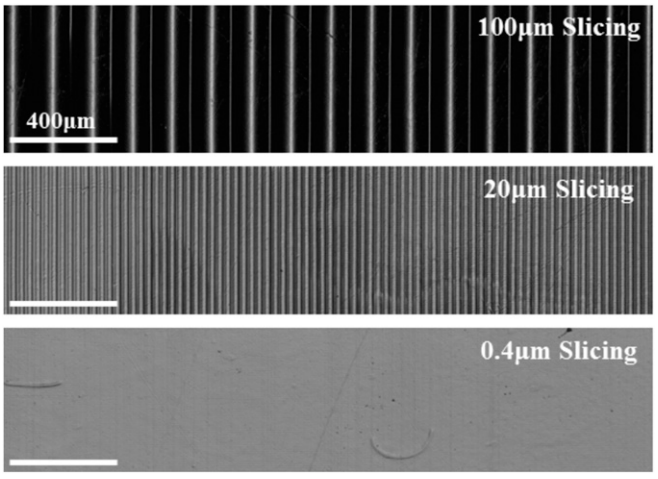

Fig. 3. Intensity images of the open book benchmark obtained with OLS noncontact profilometry. A scanning laser was used to obtain intensity profiles of the 20° page of the open book as a function of slice thickness. Laser intensity corresponds to part height where the darker regions are lower than the lighter regions. The total scanned length was held constant.

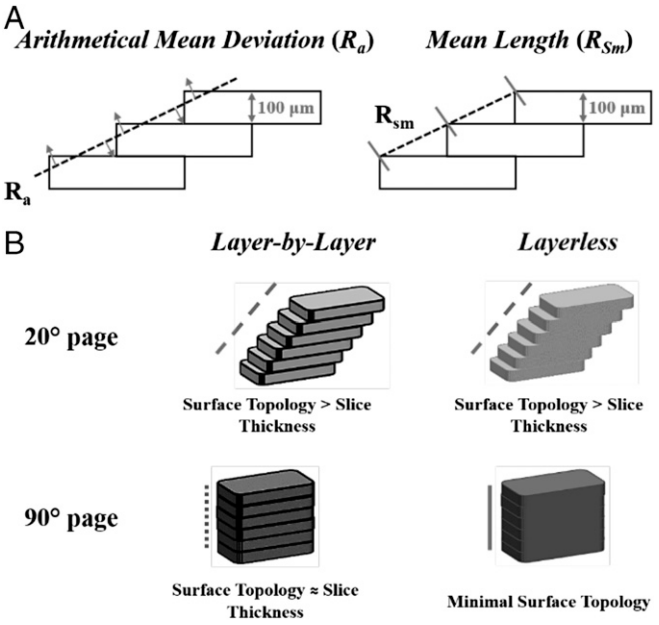

Fig. 4. Illustrations of theoretical differences in surface topology induced by AM technique. (*A*) Illustration of the two surface roughness parameters used in topological analysis. (*B*) The theoretical surface topological effects imparted by a layer-by-layer (SL) and a layerless (CLIP) fabrication approaches. The 20° for both approaches should theoretically yield similar surface effects. Therefore, the 90° page is the defining feature between layered and layerless fabrication due to its respective dependence and independence on input slice thickness.

noncontact profilometry. The changing effective slicing height, imparted by the changing angle of the open book, was corrected for using Eq. **1** to calculate the experimental step height, as shown in Table 1. This step height scales with the input slicing conditions and the mean deviation from theoretical is representative of the Z accuracy of the printer configuration. It can therefore be concluded that the observed staircasing effect is solely dependent on the input slice thickness.

$$\text{Experimental Step Height} = \cos(70) \times R_{Sm} \quad [1]$$

To ensure that the measured surface topology was due to the printed part and not the residual monomer, the soluble fraction was removed. Results from gel fraction determination, shown in Fig. S4, indicate that changing slicing condition yields no significant change in the gel fraction of the open book, and thus the polymer cross-linking of the part is unaffected by CAD file processing. The roughness was evaluated both before and after soluble fraction removal to determine the true surface topology. Roughness data after soluble fraction removal are reported in Table 1. Therefore, it can be concluded that observed "layering" in CLIP is solely imparted

Table 1. Roughness values obtained for each slice thickness condition

Slice thickness, µm	R_{Sm}, µm	R_a, µm: 90°	R_a, µm: 20°	Experimental step height, µm
100	145.65 ± 0.42	0.006 ± 0.005	13.780 ± 0.790	92.23 ± 6.01
20	28.74 ± 0.22	0.006 ± 0.005	0.820 ± 0.030	18.20 ± 1.19
0.4	0.72 ± 0.06	0.005 ± 0.005	0.012 ± 0.004	0.45 ± 0.05

Open book benchmark pages were evaluated for surface topology using OLS noncontact profilometry as a function of slice thickness following gel fraction removal. Each measurement represents $n = 3$ benchmarks with $n = 6$ measurements per imaging length. The experimental step height was calculated for the 20° page and accounts for the effective slicing due to the changing page angle. Propagation of error was accounted for in the experimental step height determination and includes uncertainties pertaining to R_{Sm} measurements and CLIP fabrication accuracy at inclines (*Supporting Information* and Figs. S2 and S3).

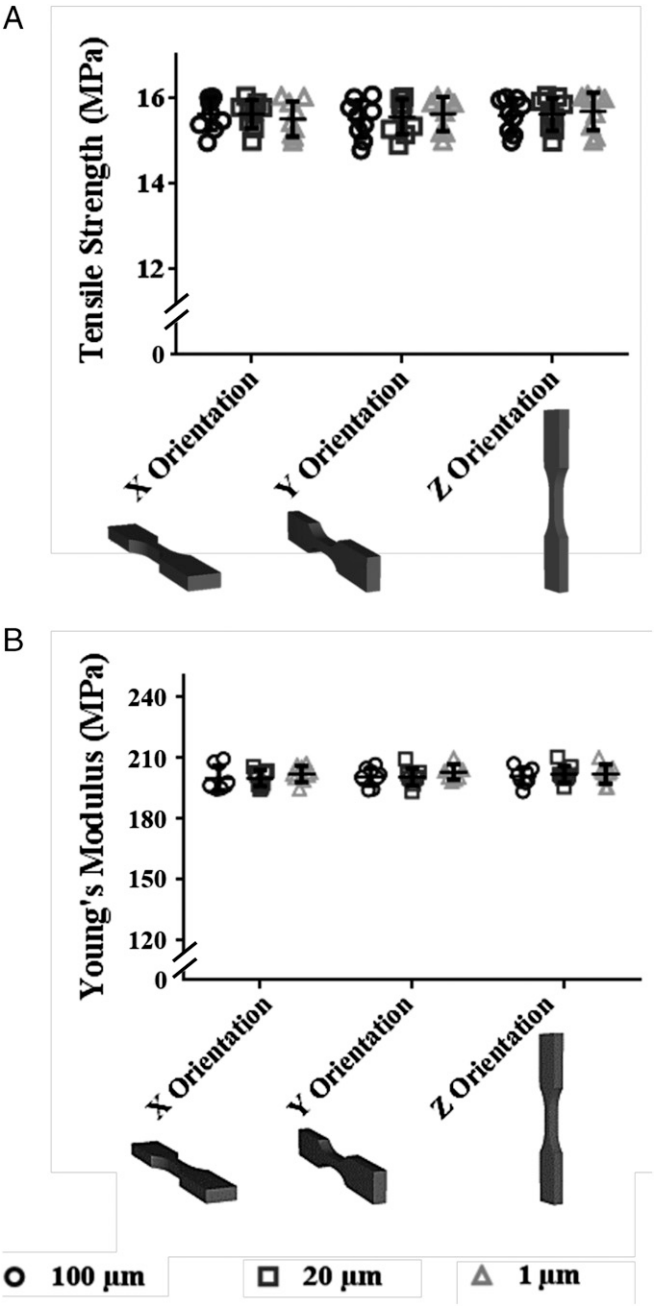

Fig. 5. Mechanical properties of fabricated parts. (*A*) Tensile strength as a function of printing orientation and slicing parameters with $n = 9$ per slicing condition per build orientation. (*B*) Young's modulus as a function of printing orientation and slicing parameters with $n = 9$ slicing condition per build orientation. No statistical difference was found using one-way ANOVA among the slicing conditions or among the fabrication orientations.

by the slice thickness and represents a purely surface topological effect rather than interfacial separations within the bulk of the part.

The mechanical properties of CLIP fabricated parts were investigated using the optimized printing parameters to explore bulk properties as a function of slice thickness and build orientation. A theoretical indicator of layerless fabrication is azimuthal independence of tensile strength and Young's modulus. This independence indicates the absence of an inherently weak axis imparted in the build direction. Both acrylate and epoxy-based SL resin systems demonstrate mechanical properties as a function of slice layer thickness (28). To provide further evidence of layerless fabrication, mechanical tests were conducted using ASTM type V dog bones printed on the three primary azimuths (Fig. 5). Tests were conducted in accordance to ASTM D638 and dog bones were fabricated with both changing azimuth and changing input slice thickness. The resulting tensile strengths and Young's moduli show no statistical difference within slice thickness or orientation. This serves as further evidence that CLIP parts are layerless and monolithic in structure. It should be noted that the resin system (trimethylolpropane triacrylate, TMPTA) used was chosen because it is a highly reactive acrylate-based system and therefore would serve as an appropriate probe of the CLIP mechanism. Typically, TMPTA functions as a cross-linking agent in resin formulation and is therefore typically only used in relatively low weight percent amounts (42). Therefore, the authors were unable to find evidence of similar studies in existing literature to confirm bulk mechanical properties of the resin formulation used or to serve as comparison with other AM platforms.

In summary, CLIP uses oxygen inhibition to enable continuous fabrication that yields truly layerless parts. These parts have improved surface finish without sacrificing build time as well as isotropic mechanical properties enabling fabrication of large overhangs, as in the case of the open book benchmark. The ability to additively manufacture parts that are layerless and monolithic using CLIP is a key step for AM to move out of the realm of rapid prototyping and into manufacturing. This paradigm shift is due to both the fast production times imparted by the continuity of the CLIP printing process as well as the final part quality both in terms of isotropic mechanical properties and smooth, layerless surface finish.

Materials and Methods

Resin Formulation. Resin reagents obtained through Sigma Aldrich were TMPTA, diphenyl(2,4,6trimethylbenzoyl)phosphine oxide (DPO), and 2-(3′-tert-butyl-2′-hydroxy-5′-methylphenyl)-5-chlorobenzotriazole (BLS1326). The base resin was formulated using TMPTA + 1.0 wt % DPO and then modified by addition of 0.03 wt % UV absorber (BLS1326) to tune the cure depth.

Part Fabrication Parameters. CAD files encoding "open book" parts were designed in SolidWorks to contain overhangs at 20, 30, 40, 50, 60, 70, 80, and 90° with dimensions of 3.5- × 5.0- × 1.0-mm base with 0.25- × 2.50- × 20-mm "pages." The resulting file was sliced for a 2D file output (.SVG) using parameters of 100-, 20-, and 0.4-μm slicing. Parts were produced continuously using 4.25 mW/cm^2 light intensity at 370-nm LED peak wavelength. The resin formulation used was TMPTA:DPO:BLS1326 99.27:0.72:0.01 mol % by acrylate functional group (TMPTA + 1.0 wt % DPO + 0.03 wt % BLS1326). Open book parts were produced at a speed of 40 mm/h with a total production time of 30.2 min. Dog bones were produced to conform to ASTM D638 guidelines for the type V parameters. The CAD file was generated in SolidWorks in the X orientation and then modified in B9Creator to obtain the Y and Z orientations. A total of 81 dog bones were produced to encompass the X, Y, and Z orientations with slice thickness of 100, 20, and 1 μm in triplicate with nine replicates for each condition. Both open book benchmarks and dog bones were fabricated on CLIP technology supplied by Carbon, Inc. Light intensity was measured using a Dymax AccuCal by Dymax Corporation at 3-mm aperture in light intensity mode.

Environmental Scanning Electron Microscope Imaging. An environmental scanning electron microscope (ESEM) with an FEI Quanta 200 field emission gun was used to obtain micrographs of the printed parts sputter coated with 1.2 nm of Au/Pt. Imaging was carried out in high vacuum mode with appropriate magnification.

Surface Roughness Analysis. Scanning laser images and surface roughness analysis was obtained using an Olympus LEXT OSL4000. Open book benchmarks with slice thicknesses of 100, 20, and 0.4 μm were analyzed for surface roughness both before and after soluble fraction removal. The 90° and 20° pages of the benchmark were removed from the base and scanned along the slope. The scanning parameters were validated by comparing fast and fine mode scanning. It was determined that the optimal scanning parameters were XYZ fast scan with a 20× objective using 1 × 5 stitch encompassing a 2,376- × 646-μm^2 area. The image obtained was treated with a "tilt" noise correction to counter the inherent slope of the open book page. A total of six line roughness measurements were obtained per sample and the R_a and R_{sm} were quantified.

Mechanical Testing. ASTM type V dog bones were measured with a micrometer for total length, length of neck, thickness, and width before mechanical testing (Table S1). Mechanical testing was conducted using an Instron 5566 with a cross-head speed of 1 mm/min at 25 °C to achieve the break at roughly 60 s, which is in accordance to the 30 s–5 min outlined in ASTM D638. Tensile strength was calculated using the maximum load of the stress/strain curve. Young's modulus was calculated using the linear portion of the stress/strain curve.

Acknowledgments

We thank Carbon, Inc. for supporting this research; Chris Dunkley (Olympus) for his training and contribution with the LEXT OLS400 confocal imaging; and Ashley Johnson, Gregory Robbins, and Chris Luft for their contributions to scientific discussions.

1 Huang SH, Liu P, Mokasdar A, Hou L (2013) Additive manufacturing and its societal impact: A literature review. *Int J Adv Manuf Technol* 67(5–8):1191–1203.
2 Lipson H, Kurman M (2013) *Fabricated : The New World of 3D Printing* (Wiley, Somerset, NJ).
3 Bartolo PJ (2011) *Stereolithography: Materials, Processes and Applications* (Springer, New York).
4 Sun C, Fang N, Wu DM, Zhang X (2005) Projection micro-stereolithography using digital micro-mirror dynamic mask. *Sens Actuators A Phys* 121(1):113–120.
5 Caulfield B, McHugh PE, Lohfeld S (2007) Dependence of mechanical properties of polyamide components on build parameters in the SLS process. *J Mater Process Technol* 182(1–3):477–488.
6 Ahn S-H, Montero M, Odell D, Roundy S, Wright PK (2002) Anisotropic material properties of fused deposition modeling ABS. *Rapid Prototyping J* 8(4):248–257.
7 Melchels FPW, Feijen J, Grijpma DW (2010) A review on stereolithography and its applications in biomedical engineering. *Biomaterials* 31(24):6121–6130.
8 Peltola SM, Melchels FPW, Grijpma DW, Kellomäki M (2008) A review of rapid prototyping techniques for tissue engineering purposes. *Ann Med* 40(4): 268–280.
9 Yagci Y, Jockusch S, Turro NJ (2010) Photoinitiated polymerization: Advances, challenges, and opportunities. *Macromolecules* 43:6245–6260.
10 Schuster M, et al. (2007) Evaluation of biocompatible photopolymers I: Photoreactivity and mechanical properties of reactive diluents. *J Macromol Sci Part A* 44(5): 547–557.
11 O'Neill PF, et al. (2014) Advances in three-dimensional rapid prototyping of microfluidic devices for biological applications. *Biomicrofluidics* 8(5):052112.
12 Whitesides GM (2006) The origins and the future of microfluidics. *Nature* 442(7101):368–373.
13 Erkal JL, et al. (2014) 3D printed microfluidic devices with integrated versatile and reusable electrodes. *Lab Chip* 14(12):2023–2032.
14 Oropallo W, Piegl LA (2016) Ten challenges in 3D printing. *Eng Comput* 32(1):135–148.
15 Mellor S, Hao L, Zhang D (2014) Additive manufacturing: A framework for implementation. *Int J Prod Econ* 149:194–201.

16 Campbell T, Williams C, Ivanova O, Garret B (2012) Could 3D printing change the world? Technologies, potential, and implications of additive manufacturing (Atlantic Council, Washington, DC).
17 Cheah CM, et al. (1997) Characteristics of photopolymeric material used in rapid prototypes Part II. Mechanical properties at post-cured state. *J Mater Process Technol* 67(1–3):46–49.
18 Mansour S, Gilbert M, Hague R (2007) A study of the impact of short-term ageing on the mechanical properties of a stereolithography resin. *Mater Sci Eng A* 447(1–2):277–284.
19 Kim GD, Oh YT (2008) A benchmark study on rapid prototyping processes and machines: Quantitative comparisons of mechanical properties, accuracy, roughness, speed, and material cost. *Proc Inst Mech Eng Part B* 222:201–215.
20 Guo N, Leu MC (2013) Additive manufacturing: Technology, applications and research needs. *Front Mech Eng* 8(3):215–243.
21 Wong KV, Hernandez A (2012) A review of additive manufacturing. *ISRN Mech Eng* 2012:1–10.
22 Cheah CM, et al. (1997) Characteristics of photopolymeric material used in rapid prototypes Part I. Mechanical properties in the green state. *J Mater Process Technol* 67:41–45.
23 Pandey PM, Reddy NV, Dhande SG (2003) Slicing procedures in layered manufacturing: A review. *Rapid Prototyping J* 9:274–288.
24 Paul R, Anand S (2015) A new Steiner patch based file format for additive manufacturing processes. *Comput Des (Winchester)* 63:86–100.
25 Hague R, Mansour S, Saleh N, Harris R (2004) Materials analysis of stereolithography resins for use in rapid manufacturing. *J Mater Sci* 39(7):2457–2464.
26 Dulieu-Barton J, Fulton M (2000) Mechanical properties of a typical stereolithography resin. *Strain* 36(2):81–87.
27 Corcione CE, Greco A, Maffezzoli A (2004) Photopolymerization kinetics of an epoxy-based resin for stereolithography. *J Appl Polym Sci* 92(6):3484–3491.
28 Chockalingam K, Jawahar N, Chandrasekhar U (2006) Influence of layer thickness on mechanical properties in stereolithography. *Rapid Prototyping J* 12(2): 106–113.
29 Tumbleston JR, et al. (2015) Continuous liquid interface production of 3D objects. *Science* 347(6228):1349–1352.
30 O'Brien AK, Bowman CN (2006) Modeling the effect of oxygen on photopolymerization kinetics. *Macromol Theory Simul* 15(2):176–182.
31 Shawkat ES, Shortall AC, Addison O, Palin WM (2009) Oxygen inhibition and incremental layer bond strengths of resin composites. *Dent Mater* 25(11):1338–1346.
32 Ligon SC, Husár B, Wutzel H, Holman R, Liska R (2014) Strategies to reduce oxygen inhibition in photoinduced polymerization. *Chem Rev* 114(1):557–589.
33 Wight FR (1978) Oxygen inhibition of acrylic photopolymerization. *J Polym Sci Lett Ed* 16(1):121–127.
34 Dendukuri D, et al. (2008) Modeling of oxygen-inhibited free radical photopolymerization in a PDMS microfluidic device. *Macromolecules* 41:8547–8556.
35 Andrzejewska E (2001) Photopolymerization kinetics of multifunctional monomers. *Prog Polym Sci* 26(4):605–665.
36 Moylan S, Slotwinski J, Cooke A, Jurrens K, Donmez MA (2012) Proposal for a standardized test artifact for additive manufacturing machines and processes. *Proceedings of the Solid Freeform Fabrication Symposium* (Laboratory for Freeform Fabrication, University of Texas at Austin, Austin, TX), pp 902–920.
37 Castillo L (2005) Study about the rapid manufacturing of complex parts of stainless steel and titanium (TNO Industrial Technology, Delft, The Netherlands).
38 Liravi F, Das S, Zhou C (2015) Separation force analysis and prediction based on cohesive element model for constrained-surface stereolithography processes. *Comput Des (Winchester)* 69:134–142.
39 Luis Perez CJ, Vivancos J, Sebastián MA (2001) Surface roughness analysis in layered forming processes. *Precis Eng* 25:1–12.
40 Strano G, Hao L, Everson RM, Evans KE (2013) Surface roughness analysis, modelling and prediction in selective laser melting. *J Mater Process Technol* 213(4): 589–597.
41 Byun HS, Lee KH (2006) Determination of optimal build direction in rapid prototyping with variable slicing. *Int J Adv Manuf Technol* 28:307–313.
42 Shaffer S, Yang K, Vargas J, Di Prima MA, Voit W (2014) On reducing anisotropy in 3D printed polymers via ionizing radiation. *Polym (United Kingdom)* 55(23): 5969–5979.
43 Lee TY, Guymon CA, Jönsson ES, Hoyle CE (2004) The effect of monomer structure on oxygen inhibition of (meth)acrylates photopolymerization. *Polymer (Guildf)* 45(18):6155–6162.